Effect of rheological properties on drag reduction in turbulent boundary layer flow

Shinji Tamano,[1,a)] Motoyuki Itoh,[1] Shintaro Hotta,[2] Kazuhiko Yokota,[1] and Yohei Morinishi[1]
[1]*Graduate School of Engineering, Nagoya Institute of Technology, Gokiso-cho, Showa-ku, Nagoya, Aichi 466-8555, Japan*
[2]*Toyota Motor Corporation, 1 Toyota-cho, Toyota, Aichi 471-8571, Japan*

(Received 14 January 2009; accepted 17 April 2009; published online 13 May 2009)

Direct numerical simulation of a zero-pressure gradient drag-reducing turbulent boundary layer of viscoelastic fluids was systematically performed at the momentum-thickness Reynolds number $\mathrm{Re}_{\theta_0}=500$ and Weissenberg number $\mathrm{We}=25$ using constitutive equation models such as the Oldroyd-B, the finitely extensible nonlinear elastic Peterlin model at the maximum chain extensibility parameters $L^2=100$, 1000, and 10 000, and the Giesekus model at the mobility factors $\alpha=0.01$, 0.001, and 0.0001, where the ratios of solvent viscosity to zero shear rate solution viscosity, β, were 0.9, 0.99, and 0.999. For the case that the elongational viscosity for the steady elongational flow was identical, the streamwise variation in the drag reduction (DR) was thoroughly investigated, and then the effects of rheological properties such as the elongational and shear viscosities and the first and the second normal stress differences on DR were clarified. It is found that the streamwise profile of DR shifts downstream with the decrease in the first normal stress difference. The shear-thinning property and the first normal stress difference slightly affect the maximum DR, while the decrease in the magnitude of the second normal stress difference results in the decrease in the maximum DR. © *2009 American Institute of Physics*. [DOI: 10.1063/1.3137163]

I. INTRODUCTION

It is well known that a drag reduction (DR) can be obtained for wall-bounded turbulent flows of viscoelastic fluids such as the dilute polymer and surfactant solutions. In the past decade, numerous direct numerical simulations (DNSs) have been performed to investigate the drag-reducing viscoelastic turbulent flows using constitutive equation models such as the finitely extensible nonlinear elastic Peterlin (FENE-P) model, Oldroyd-B model, and Giesekus model. These DNS studies on drag-reducing turbulent channel flow have revealed the effect of viscoelastic stress on velocity fields and have contributed to the understanding of the drag-reducing mechanism of viscoelastic fluids, as reported in a recent review.[1] For the drag-reducing turbulent boundary layer flow, however, the previous DNSs (Refs. 2–4) have not sufficiently predicted the existing experimental measurements[5–7] including the rheological properties, which have revealed that the streamwise variations in the turbulence statistics and structures were fairly complex. The main reason for this is attributed to the difficulty of accurate measurements of rheological properties, except for the shear viscosity, for the dilute aqueous polymer and surfactant solutions. To our knowledge, there are some available measurement data on the shear viscosity and the first normal stress difference (the relaxation time),[8–14] while there are only a few available data on the extensional viscosity.[11–13,15,16]

Lu *et al.*[11,12] and Lin *et al.*[13] reported that for the surfactant solution with the constant shear viscosity and the zero first normal stress difference, the large DR could be obtained, the entangled network structures of threadlike micelles were observed, and the elongational viscosity and the Trouton ratio were extremely high compared to the Newtonian fluid. On the other hand, Kawaguchi *et al.*[16] reported that the elongational viscosity of very dilute drag-reducing cationic surfactant solution was almost the same as that of water. Since there are issues with experimental characterization of drag-reducing solutions, it is quite difficult or impossible, so far, to perform the DNS of the drag-reducing wall-bounded turbulent flows of viscoelastic fluids whose rheological parameters exactly correspond to those of the real drag-reducing turbulent flows, although a lot of understanding has been established over ten years of the DNS work. A new work on the rheology of drag-reducing solutions, which focuses on applying more realistic parameters to the Oldroyd-B, FENE-P, Giesekus, or other models, would be required. Such an attempt was done by Paschkewitz *et al.*,[17] who experimentally and numerically investigated the DR in a turbulent boundary layer using a rigid rodlike polymer. There have been also several DNS studies on the effects of rheological parameters of drag-reducing turbulent channel flows using the existing constitutive equation models, which claimed that the elongational viscosity and Weissenberg number were key parameters for the DR.[18–21] Until now, however, the relation between rheological properties and DR is not fully understood.

Regarding the DNS of drag-reducing turbulent boundary layer flow of viscoelastic fluids, recently, Dimitropoulos *et al.*[2] performed a DNS of a polymer-induced drag-reducing zero-pressure gradient turbulent boundary layer flow of ho-

[a)]Telephone: +81-52-735-5609. Fax: +81-52-735-5247. Electronic mail: tamano.shinji@nitech.ac.jp.

mogeneous polymer solutions using the FENE-P model and found that the larger DR could be obtained at a larger Weissenberg number as well as for the turbulent channel flows. The drag-reducing effect in turbulent boundary layer flow of inhomogeneous polymer solutions was also investigated by Dimitropoulos *et al.*[3] Tamano *et al.*[4] reported the DNS results of drag-reducing turbulent boundary layer in viscoelastic fluids using the Oldroyd-B and Giesekus models and found that the larger elongational viscosity was important for the larger DR as well as the turbulent channel flow. However, the effects of rheological parameters such as the elongational and shear viscosities and the first and the second normal stress differences on the streamwise variation in DR of the drag-reducing turbulent boundary layer flows have not been systematically investigated. Even for the drag-reducing turbulent channel flow, to our knowledge, there has not been a comprehensive study on the effects of these rheological properties on DR.

In the present study, we perform the DNS of a zero-pressure gradient turbulent boundary layer of a drag-reducing homogeneous viscoelastic fluid using constitutive equation models such as the Oldroyd-B, FENE-P, and Giesekus models in which the rheological properties are different and investigate the effects of the rheological properties such as the elongational and shear viscosities and the first and the second normal stress differences on DR. We systematically performed the DNS for the Oldroyd-B, the FENE-P model at the maximum chain extensibility parameters $L^2=100$, 1000, and 10 000, and the Giesekus model at the mobility factors $\alpha=0.01$, 0.001, and 0.0001 at the ratios of solvent viscosity to zero shear rate solution viscosity $\beta=0.9$, 0.99, and 0.999. We also compared the DNS data obtained, focusing on the case that the elongational viscosity for the steady elongational flow is identical, since there are many combinations of rheological parameters and many previous studies claimed that the elongational viscosity was the most important rheological property for large DR. The present approach focusing on comparison at the same elongational viscosity is the first attempt to date to understand the effects of rheological properties on DR.

Moreover, we investigated the effects of the rheological properties on the streamwise variations in the local maxima of turbulence statistics, which has not been investigated in the previous study. It has been reported that the dependence of turbulence intensity of the velocity fluctuation on DR was complex.[7] In particular, the relation between the maximum streamwise turbulence intensity and DR remains unclear.[4] In addition, the streamwise variation in the local maximum of the trace of the viscoelastic stress components, which represents the magnitude of the polymer elongation, was investigated to clarify the relation between velocity and viscoelastic stress fields.

In addition to the effects of the rheological properties investigated here, the effects of the Weissenberg and Reynolds numbers are important for the drag-reducing wall-bounded turbulent flow. Readers are referred to the studies of Housiadas and Beris[22] and Li *et al.*[20] in which the effects of the Weissenberg and Reynolds numbers on DR and the turbulence statistics for turbulent channel flow are thoroughly examined using the DNS data. We also present some results concerning the effect of the Weissenberg number, i.e., the relaxation time on the streamwise variation in DR for the turbulent boundary layer flow with the FENE-P model, in Sec. IV E.

The present paper is arranged as follows. The fundamental equations for the present study are presented in Sec. II. The details of the present DNS data are provided in Sec. III. In Sec. IV, at the same elongational viscosity, the effects of rheological properties on the streamwise variation in DR are examined using the present numerical simulation results. Key results are summarized and conclusions are given in Sec. V.

II. FUNDAMENTAL EQUATIONS

The nondimensional governing equations for the incompressible viscoelastic flow are continuity and momentum equations:

$$\frac{\partial u_i}{\partial x_i}=0, \tag{1}$$

$$\frac{\partial u_i}{\partial t}+\frac{\partial u_i u_j}{\partial x_j}=-\frac{\partial p}{\partial x_i}+\frac{1-\beta}{\mathrm{Re}_{\theta_0}}\frac{\partial E_{ij}}{\partial x_j}+\frac{\beta}{\mathrm{Re}_{\theta_0}}\frac{\partial^2 u_i}{\partial x_j\,\partial x_j}, \tag{2}$$

where u_i is the velocity component, p is the pressure, x_i is a spatial coordinate, t is the time, and E_{ij} is the viscoelastic stress component. In this paper, x_1 (x), x_2 (y), and x_3 (z) directions are streamwise, wall normal, and spanwise, respectively. $\beta=\eta_s/\eta_0$ is the ratio of solvent viscosity η_s to zero shear rate solution viscosity η_0. The nondimensional constitutive equation for conformation tensor c_{ij} is as follows:

$$\frac{\partial c_{ij}}{\partial t}+u_k\frac{\partial c_{ij}}{\partial x_k}-\frac{\partial u_i}{\partial x_k}c_{kj}-\frac{\partial u_j}{\partial x_k}c_{ik}=-E_{ij}-\alpha\,\mathrm{We}\,E_{jk}E_{ki}, \tag{3}$$

where the mobility factor α is zero for the Oldroyd-B and FENE-P models and $0<\alpha<1$ for the Giesekus model.[19] The mobility factor α is related to the extensibility of the polymer chains. The viscoelastic stress component is related to the conformation tensor,

$$E_{ij}=\frac{fc_{ij}-\delta_{ij}}{\mathrm{We}}, \tag{4}$$

where the Peterlin function f is unity for the Oldroyd-B and Giesekus models. For the FENE-P model, f is defined by

$$f=\frac{L^2}{L^2-\mathrm{Tr}(c_{ij})}, \tag{5}$$

where L represents the maximum extension of polymer.[19]

In this study, the inflow condition for the boundary layer is given by the method proposed by Lund *et al.*,[23] so that the computational domain is divided into the main part and driver part in which the inflow condition for the main part is obtained. In the present study, the nondimensional computa-

tional parameters are the momentum-thickness Reynolds number Re_{θ_0} and the Weissenberg number We, which are defined as follows:

$$\mathrm{Re}_{\theta_0} = \frac{\rho U_e \theta_0}{\eta_0}, \tag{6}$$

$$\mathrm{We} = \frac{\lambda U_e}{\theta_0}, \tag{7}$$

where U_e is the free-stream velocity, θ_0 is the momentum thickness at the inlet plane of the driver part, ρ is the density, and λ is the relaxation time.

III. NUMERICAL METHOD AND CONDITIONS

The second-order accurate finite difference scheme on a staggered grid is used. The velocity components are discretized on the grid cell edges, whereas the pressure and all the components of viscoelastic stress tensor E_{ij} and conformation tensor c_{ij} are defined at the center of each cell. The coupling algorithm of the discrete continuity and momentum equations (1) and (2) is based on the second-order splitting method.[24] The resulting discrete Poisson equation for the pressure is solved using the successive over-relaxation method and biconjugate gradients stabilized method[25] after fast Fourier transforming in the periodic (z) direction. The second-order upwind difference scheme is used for the polymer-stress convection term $u_k \partial c_{ij}/\partial x_k$ in Eq. (3). An artificial diffusion κ^* We $\partial^2 c_{ij}/\partial x_j^2$ is added in Eq. (3) to prevent the numerical instability, where κ^* is the dimensionless artificial diffusion factor. The semi-implicit time marching algorithm is used where the diffusion term in the wall-normal direction is treated implicitly with the Crank–Nicolson scheme, and the third-order Runge–Kutta scheme is used for all other terms.

The nonslip boundary condition ($u=v=w=0$) is applied on the wall. The boundary conditions on the top surface of the computational domain are $\partial u/\partial y=0$, $v=U_e d\delta^*/dx$, and $\partial w/\partial y=0$, where δ^* is the boundary layer displacement thickness. A convective boundary condition,

$$\frac{\partial u_i}{\partial t} + U_e \frac{\partial u_i}{\partial x} = 0, \tag{8}$$

is used at the outlet plane. The inflow condition is generated using the recycle method.[23] In the present study, the velocity field data at the streamwise center of the driver part provide inflow data at the inlet of the main part. The boundary conditions for viscoelastic stress components are given by solving the constitutive equations at the wall with the velocity boundary conditions satisfied, except for the inlet boundary at the main part in which the Newtonian velocity data are imposed directly.[2,4] Note that the inlet boundary condition used here makes the results of relevance primarily at a very long distance and only if they are stationary. The periodic boundary conditions for velocity and viscoelastic stress components are imposed in the spanwise direction. The statistically steady Newtonian velocity data are used as the initial condition for the Oldroyd-B model. Moreover, the statistically steady velocity and viscoelastic stress data for the Oldroyd-B model are used as the initial condition for the FENE-P and Giesekus models.

In the present study, the momentum-thickness Reynolds number Re_{θ_0} is 500 and the Weissenberg number We is 25. The size of the computational domain for the present simulations is equal to $(L_x \times L_y \times L_z) = (200\theta_0 \times 30\theta_0 \times 20\pi\theta_0/3)$ in the streamwise, wall-normal, and spanwise directions, respectively. The grid size is $(N_x \times N_y \times N_z) = (256 \times 64 \times 64)$. The grid spacing in the x and z directions is uniform, and the wall-normal grids are given by a hyperbolic tangent stretching function. The present spatial resolution is comparable to that of previous DNS attempts[2,4] for the corresponding drag-reducing turbulent boundary layer with the same spatial discretization method. In the driver part, the computational domain and grid size are $(100\theta_0 \times 30\theta_0 \times 20\pi\theta_0/3)$ and $(128 \times 64 \times 64)$, respectively. The present turbulence statistics are obtained by averaging over space (spanwise direction) and time of over $1000\theta_0/U_e$ after the turbulent flow becomes stationary, where the time increment $\Delta t U_e/\theta_0$ is 0.008 for the Oldroyd-B, FENE-P, and Giesekus models and 0.02 for Newtonian fluid. In this paper, $\bar{}$ and $'$ represent the time-space (spanwise direction) average and the deviation, respectively. The $^+$ represents the variables normalized by wall variables. The dimensionless artificial diffusion factor κ^* is set to be 0.01. The code verification of the DNS for the Oldroyd-B and Giesekus models was done in our previous study.[4] The code verification of the DNS for the FENE-P model was checked in the drag-reducing turbulent channel flow at the friction Reynolds number of 125 and the friction Weissenberg number of 50 (see Ref. 18), in addition to comparing with the DNS data of Dimitropoulos *et al.*[2] for the drag-reducing turbulent boundary layer flow.

IV. RESULTS

A. DR for the Oldroyd-B model

Figures 1(a) and 1(b) show the elongational viscosity $\eta_E/(3\eta_0)$ and the first normal stress difference coefficient $\psi_1/(2\eta_0\lambda)$, which are given by Eqs. (A1) and (A7) in Appendix A, for the Oldroyd-B model at the shear viscosity ratios $\beta=0.9$, 0.99, and 0.999. With the increase in β, i.e., approaching unity, the slope of $\eta_E/(3\eta_0)$ at $\lambda\dot{\varepsilon} \simeq 0.5$ becomes steeper, but the difference is small. The value of $\eta_E/(3\eta_0)$ becomes infinite for $\lambda\dot{\varepsilon} > 0.5$, which is independent of β. The value of $\psi_1/(2\eta_0\lambda)$ decreases with the increase in β. For the Oldroyd-B model, the shear viscosity is constant ($\eta/\eta_0=1$), and the second normal stress difference is zero, which is independent of β.

In the present DNS data on the drag-reducing turbulent boundary layer, the time-averaged maxima of the nondimensional elongational and shear rates were $\lambda\dot{\varepsilon} \simeq 1$ and $\lambda\dot{\gamma} \simeq 35$, respectively. Although these values are within the range of rheological properties presented in this study, for the turbulent boundary layer flow, they can vary in the wider range between zero and much larger values spatially and temporally, so that rheological properties would be very complex. The study on the effects of the unsteady rheological properties on the turbulent boundary layer flow is beyond the scope of the present work.

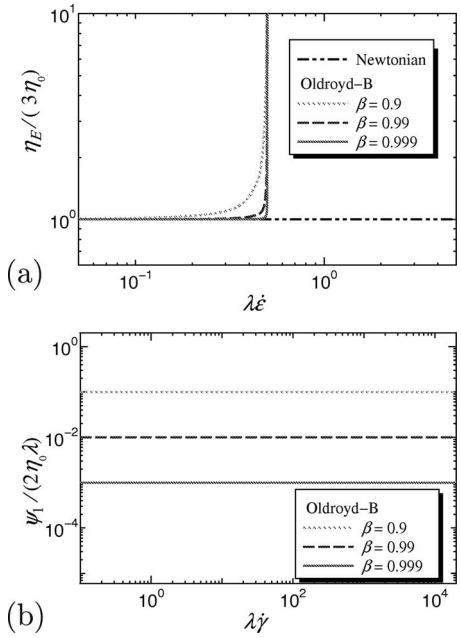

FIG. 1. Rheological properties of the Oldroyd-B model: (a) elongational viscosity and (b) the first normal stress difference coefficient.

Figure 2 shows the streamwise variation in the DR ratio, which is defined as follows:

$$\mathrm{DR} = \frac{C_{f_{\mathrm{Newtonian}}} - C_{f_{\mathrm{viscoelastic}}}}{C_{f_{\mathrm{Newtonian}}}}, \tag{9}$$

where $C_{f_{\mathrm{Newtonian}}}$ and $C_{f_{\mathrm{viscoelastic}}}$ are the skin friction coefficients for Newtonian and viscoelastic fluids at the same streamwise positions. At $\beta=0.9$, 0.99, and 0.999, the positive DR is observed at $x/\theta_0>40$, $x/\theta_0>50$, and $x/\theta_0>75$, respectively, which indicates that the drag-reducing effect appears more downstream with the increase in β. Considering that with the increase in β, ψ_1 decreases [see Fig. 1(b)] and the other rheological parameters are only slightly altered, it can be concluded that the streamwise profile of DR shifts downstream with the decrease in the first normal stress difference. The reason can be explained as follows.

For the Oldryod-B model,[26] ψ_1 is represented for the steady shear flow as follows:

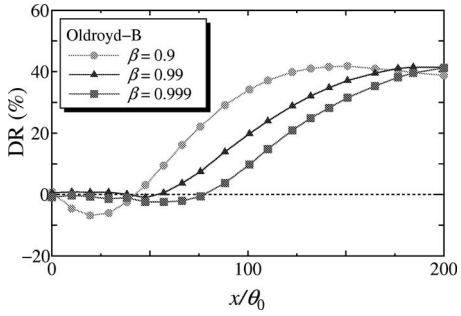

FIG. 2. Streamwise variation in DR for the Oldroyd-B model.

$$\psi_1 = 2\eta_0(\lambda - \lambda'), \tag{10}$$

where $\lambda'=\beta\lambda$ is the retardation time. At the same Weissenberg number, the relaxation time λ is constant, and λ' increases with the increase in β. Therefore, the decrease in ψ_1 corresponds to the increase in λ'.

Figure 2 also shows that the maximum DR at $\beta=0.9$ is slightly larger than those at $\beta=0.99$ and 0.999, although the difference is somewhat larger in the larger streamwise computational domain (see Appendix B in detail). This indicates that the first normal stress difference slightly affects the maximum DR.

At $\beta=0.9$, the increase in the skin friction drag (DR $<0\%$) near the inlet region may be due to the sudden change in velocity fields caused by the unrealistic effect of the inlet boundary condition in which the velocity field data of Newtonian fluid in the driver part are used directly, as pointed out in the literature.[2,4] At $\beta=0.99$ and 0.999, on the other hand, the distinct drag increase near the inlet boundary is not observed. This may be because the change in velocity fields near the inlet boundary is relatively small at $\beta=0.99$ and 0.999, which are very close to the Newtonian value ($\beta=1$).

B. DR for the FENE-P model

For the FENE-P model at the maximum extensions $L^2=100$, 1000, and 10 000 and $\beta=0.9$, 0.99, and 0.999, $\eta_E/(3\eta_0)$, η/η_0, and $\psi_1/(2\eta_0\lambda)$, which are given by Eqs. (A2), (A9), and (A10) in Appendix A, are shown in Figs. 3(a)–3(c), respectively. The second normal stress difference for the FENE-P model is zero. For the FENE-P model, at the same value of $L^2(1-\beta)$, the maximum elongational viscosity, i.e., the elongational viscosity at the infinite elongational rate, becomes identical for different combinations of β and L^2, and then the shape of the profile is also the same, as shown in Fig. 3(a). With the decrease in $L^2(1-\beta)$, the maximum elongational viscosity decreases. In this section, we investigate the relation between rheological properties and the streamwise variation in DR for three cases of $L^2(1-\beta)=1000$, 100, and 10. With the decrease in β, the shear thinning, in which the shear viscosity becomes smaller with the increase in the shear rate, becomes more distinct, i.e., the slope of the curve of the shear viscosity versus the shear rate becomes larger [Fig. 3(b)]. Figure 3(c) shows that ψ_1 becomes larger with the decrease in β at the same elongational viscosity.

Figure 4 shows the streamwise variation in DR for the FENE-P model. At $L^2(1-\beta)=100$, i.e., $(L^2,\beta)=(1000,0.9)$ and (10 000 0.99), the streamwise profile of DR shifts downstream with the increase in β. The increase in β corresponds to the decrease in the first normal stress difference and/or the reduction in the shear thinning [see Figs. 3(b) and 3(c)]. Taking account of the results for the Oldroyd-B model (see Sec. IV A), it can be deduced that the downstream shift of the curve of DR is due to the decrease in the first normal stress difference. At the same elongational viscosity, the maximum DR is almost the same for different β, which indicates that the shear-thinning property and the first normal stress differ-

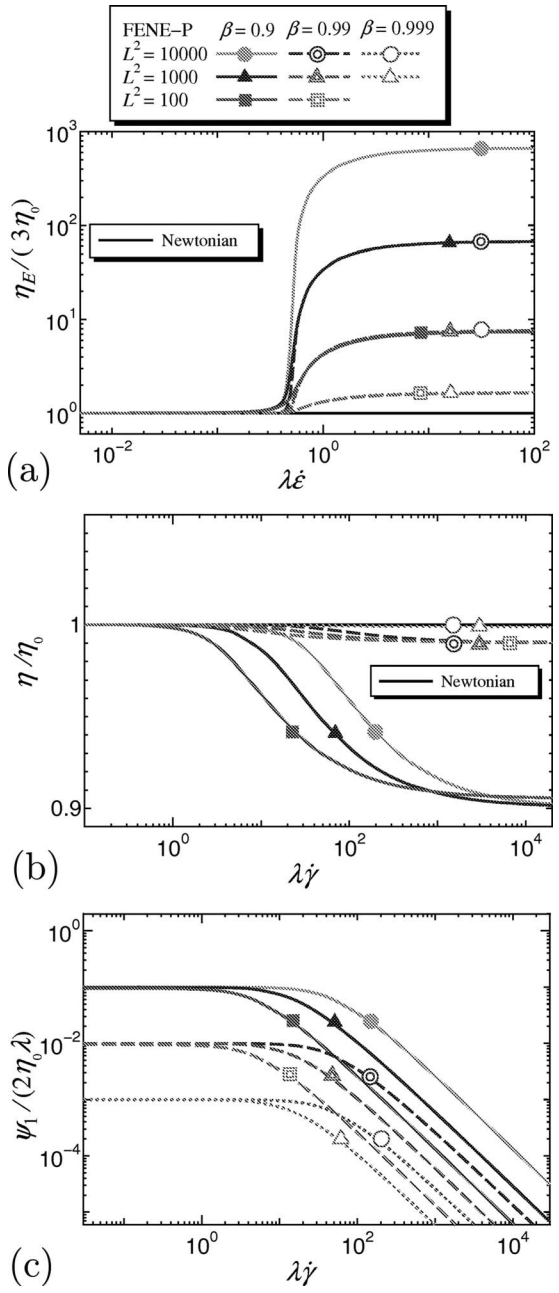

FIG. 3. Rheological properties of the FENE-P model: (a) elongational viscosity, (b) shear viscosity, and (c) the first normal stress difference coefficient.

ence only slightly affect the maximum DR. At $L^2(1-\beta)=10$, the maximum DR is relatively small and the trend observed at $L^2(1-\beta)=100$ cannot be observed.

C. DR for the Giesekus model

For the Giesekus model at the mobility factors $\alpha=0.01$, 0.001, and 0.0001 and $\beta=0.9$, 0.99, and 0.999, $\eta_E/(3\eta_0)$, η/η_0, $\psi_1/(2\eta_0\lambda)$, and the second normal stress difference coefficient $-\psi_2/(\eta_0\lambda)$, which are given by Eqs. (A5) and (A14)–(A16) in Appendix A, are shown in Figs. 5(a)–5(d), respectively. Figure 5(a) shows that the profile of the elongational viscosity is identical for different combinations of β and α at the same value of $(1-\beta)/\alpha$ for the Giesekus model.

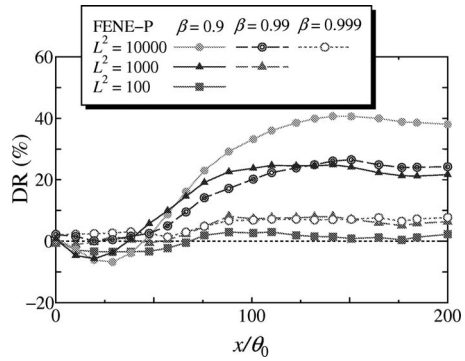

FIG. 4. Streamwise variation in DR for the FENE-P model.

In this section, we investigate the effects of rheological properties for four cases of $(1-\beta)/\alpha=1000$, 100, 10, and 1. The elongational viscosity decreases with the decrease in $(1-\beta)/\alpha$ from 1000 to 1 [Fig. 5(a)]. At the same value of $(1-\beta)/\alpha$, i.e., at the same elongational viscosity, with the decrease in β, the shear-thinning property becomes more distinct [Fig. 5(b)], and the magnitudes of ψ_1 and ψ_2 become larger [Figs. 5(c) and 5(d)].

Figure 6 shows the streamwise variation in DR for the Giesekus model. At $(1-\beta)/\alpha=100$ [$(\alpha,\beta)=(0.001,0.9)$ and $(0.0001,0.99)$], the streamwise profile of DR shifts downstream with the increase in β. As described above, for the case of the same elongational viscosity, the increase in β corresponds to the decrease in the first normal stress difference and the reduction in the shear-thinning property. Considering these rheological properties in addition to the results in Secs. IV A and IV B, it can be deduced that the downstream shift of DR is due to the decrease in the first normal stress difference. At the same $(1-\beta)/\alpha$, the maximum DR becomes smaller with the increase in β. It can be deduced that the decrease in the maximum DR with the increase in β for the Giesekus model with the same elongational viscosity is due to the decrease in the magnitude of the second normal stress difference, since the maximum DR is almost the same for the FENE-P model at a different β with the same elongational viscosity (see Fig. 4). This finding supports the numerical analysis of Renardy,[27] who claimed that the second normal stress difference played a stronger role in DR, whereas all available simulation data show it to have an auxiliary effect. However, the magnitude of the second normal stress difference is about three orders smaller than the first normal stress difference. Thus, further investigations would be needed to reveal the contribution of the second normal stress difference to DR. At $(1-\beta)/\alpha=10$, in which DR is small, the same trend can be observed but it is more unclear compared to that at $(1-\beta)/\alpha=100$.

D. Comparison of DR between FENE-P and Giesekus models

At $\beta=0.9$, for the FENE-P model at $L^2=100$, 1000, and 10 000 and the Giesekus model at $\alpha=0.01$, 0.001, and 0.0001, $\eta_E/(3\eta_0)$, η/η_0, and $\psi_1/(2\eta_0\lambda)$ are shown in Figs. 7(a)–7(c), respectively. For the case that the relation of $L^2=1/\alpha$ is satisfied, the elongational viscosity at the infinite

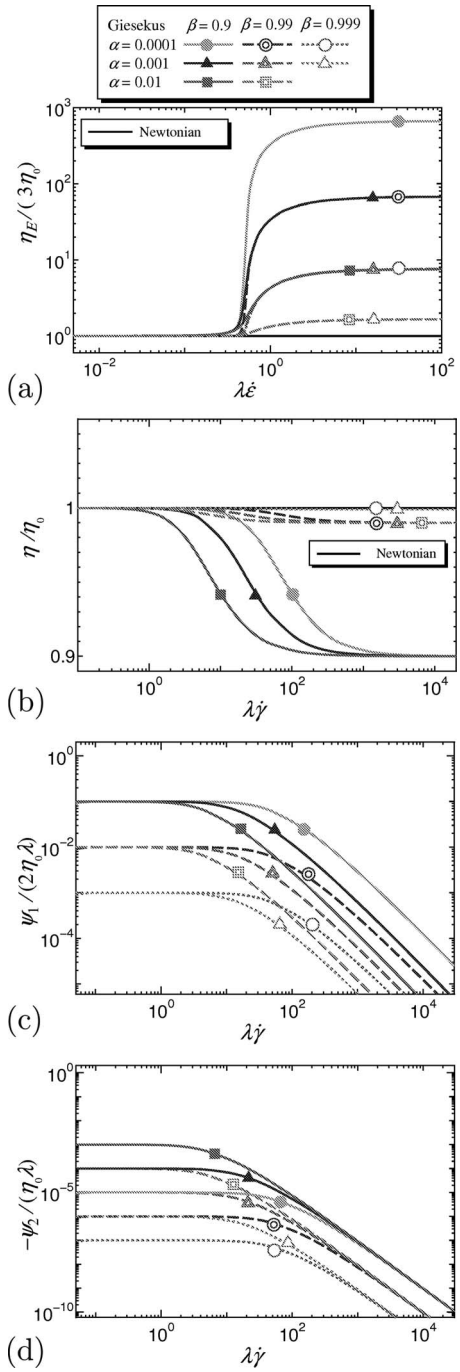

FIG. 5. Rheological properties of the Giesekus model: (a) elongational viscosity, (b) shear viscosity, (c) the first normal stress difference coefficient, and (d) the second normal stress difference coefficient.

elongational rate for both the FENE-P and Giesekus models becomes identical,[18] and thus these profiles are also the same [Fig. 7(a)]. The maximum elongational viscosity becomes larger with the decrease in α or the increase in L^2. For both the FENE-P and Giesekus models, the shear-thinning property is observed in Fig. 7(b). At the same elongational viscosity ($L^2=1/\alpha$), the shear-thinning property for the Giesekus model is more distinct than that for the FENE-P model [Fig. 7(b)]. At $L^2=1/\alpha$, the first normal stress differences for the FENE-P and Giesekus models become identical to each other [Fig. 7(c)]. The magnitude of the second normal stress difference is zero for the FENE-P model, while for the Giesekus model, it is not zero and decreases with the decrease in α at the same shear viscosity ratio ($\beta=0.9$) [see Fig. 5(d)].

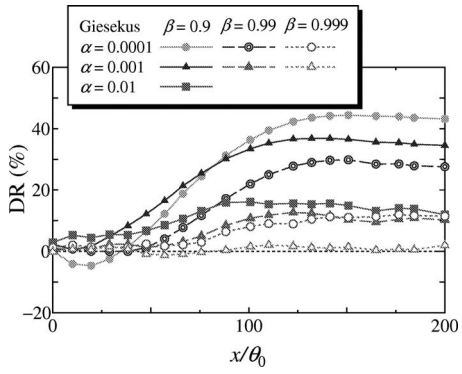

FIG. 6. Streamwise variation in DR for the Giesekus model.

Figure 8 shows the streamwise variations in DR for the FENE-P and Giesekus models at $\beta=0.9$. It is found that DR becomes larger as the elongational viscosity increases, i.e., L^2 increases for the FENE-P model and α decreases for the

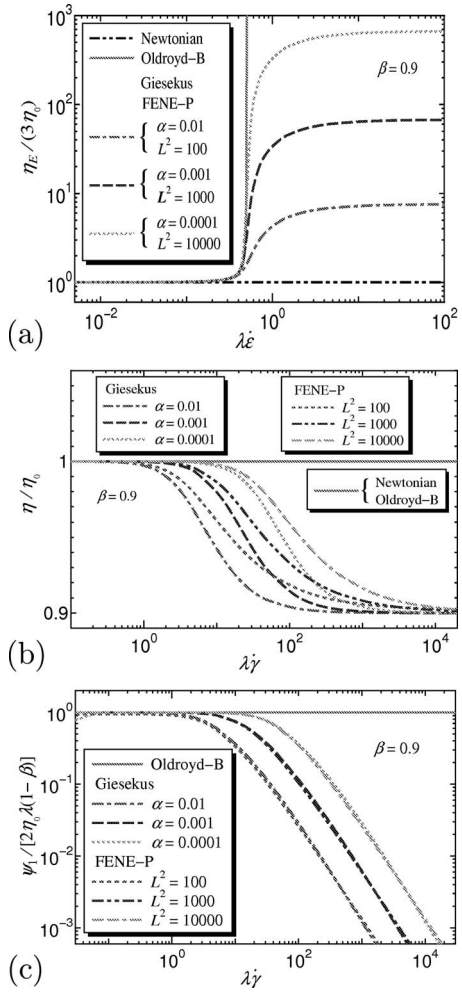

FIG. 7. Rheological properties of the FENE-P and Giesekus models at $\beta=0.9$: (a) elongational viscosity, (b) shear viscosity, and (c) the first normal stress difference coefficient.

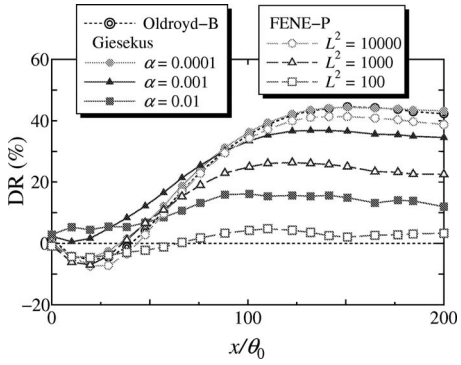

FIG. 8. Comparison of streamwise variations in DR between the FENE-P and Giesekus models at $\beta=0.9$.

Giesekus model. At the same elongational viscosity ($L^2=1/\alpha$), DR for the Giesekus model is larger than that for the FENE-P model. Two possible reasons for this can be considered. First, the shear-thinning property for the Giesekus model is more distinct than that for the FENE-P model. Second, the second normal stress difference is zero for the FENE-P model but not for the Giesekus model. For the FENE-P model at a different β, which represents the strength of the shear thinning, a visible difference in DR cannot be observed (see Sec. IV B). Therefore, it can be claimed that the reason why the maximum DR for the Giesekus model is larger than that for the FENE-P model is the existence of the second normal stress difference. The same trend has also been reported in the DNS of drag-reducing turbulent channel flow with the FENE-P and Giesekus models.[18]

E. Effect of We on DR

In order to clarify the effect of the Weissenberg number We for the FENE-P model at $\beta=0.9$ and $\mathrm{Re}_{\theta_0}=500$, the streamwise variations in DR at both We=25 and 50 are shown in Fig. 9. It is confirmed that the dependence of the streamwise variation in DR on the maximum chain extensibility parameter L^2 at We=50 is similar to that at We=25, in which the larger L^2, i.e., the larger elongational viscosity, results in the larger DR, although at the same L^2, the larger DR can be obtained at the higher Weissenberg number, as reported by Dimitropoulos *et al.*[2] For the FENE-P model at

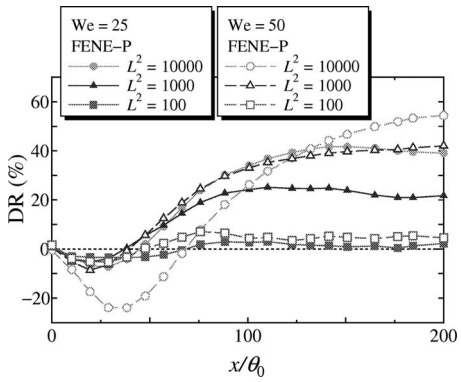

FIG. 9. Comparison of streamwise variations in DR at We=25 and 50 for the FENE-P model at $\beta=0.9$.

$L^2=10\,000$, the maximum DR at We=50 is DR=54% in the present study, while it is slightly smaller than DR≃60% in the study of Dimitropoulos *et al.*[2] at the same Weissenberg number. This difference is due to the difference in the Reynolds number, the treatment of the polymer-stress convection term, and the size of computational domain (see Appendix B for details). It is also found that at the same elongational viscosity, the streamwise profile of DR shifts downstream with the increase in We, which corresponds to the increase in the relaxation time λ.

F. Relation between DR and turbulence statistics

As noted in our previous paper,[4] the streamwise turbulence intensity does not seem to be directly related to DR. To investigate the relation between the streamwise variations in DR and turbulence statistics scaled by the friction velocity such as the streamwise turbulence intensity u^+_{rms}, the wall-normal turbulence intensity v^+_{rms}, the spanwise turbulence intensity w^+_{rms}, and the Reynolds shear stress $-\overline{u'v'}^+$, we focus on their local maxima $u^+_{\mathrm{rms\ max}}$, $v^+_{\mathrm{rms\ max}}$, $w^+_{\mathrm{rms\ max}}$, and $-\overline{u'v'}^+_{\mathrm{max}}$. Note that the wall-normal locations of local maxima are different at various streamwise locations.

Figure 10(a) shows that $u^+_{\mathrm{rms\ max}}$ for the Oldroyd-B model becomes smaller in the region from the inlet plane to near the center of the computational domain and more downstream compared to the Newtonian fluid in which $u^+_{\mathrm{rms\ max}}$ is almost constant in the whole computational domain and then becomes gradually larger in the streamwise direction. With the increase in β from 0.9 to 0.999, the streamwise variation in $u^+_{\mathrm{rms\ max}}$ shifts downstream, which corresponds to the fact that DR appears at more downstream locations with the increase in β. Note that the streamwise location of the onset for DR is more upstream compared to the location at which $u^+_{\mathrm{rms\ max}}$ becomes larger than that for the Newtonian fluid. This difference in the streamwise variations between DR and $u^+_{\mathrm{rms\ max}}$ means that, at a given streamwise location, DR seems to be unrelated to the value of $u^+_{\mathrm{rms\ max}}$. This corresponds to that no distinct relation between DR and $u^+_{\mathrm{rms\ max}}$ has been observed at the corresponding streamwise location in both the experimental and numerical studies on the drag-reducing turbulent boundary layer flow.[4,6] In addition, the lack of correspondence of DR and $u^+_{\mathrm{rms\ max}}$ observed here is consistent with the first DNS of Dimitropoulos *et al.*[2] For the FENE-P and Giesekus models, the trend of the relation between DR and $u^+_{\mathrm{rms\ max}}$ is the same as that for the Oldroyd-B model (not shown here).

Figure 10(b) shows that $v^+_{\mathrm{rms\ max}}$ for the Oldroyd-B model is much smaller than that for the Newtonian fluid in the region $x/\theta_0<100$. With the decrease in β, $v^+_{\mathrm{rms\ max}}$ decreases, except that $v^+_{\mathrm{rms\ max}}$ at $\beta=0.9$ is smaller than that for the Newtonian fluid even near the inlet region in which DR is negative. The streamwise variation in $w^+_{\mathrm{rms\ max}}$ corresponds to that in $v^+_{\mathrm{rms\ max}}$ [cf. Figs. 10(b) and 10(c)]. In the region close to the outlet plane, both $v^+_{\mathrm{rms\ max}}$ and $w^+_{\mathrm{rms\ max}}$ for the Newtonian fluid suddenly decrease. This unrealistic behavior, which is also observed for the FENE-P and Giesekus models (not shown here), is due to the effect of the outlet boundary condition given by Eq. (8). It is confirmed that the

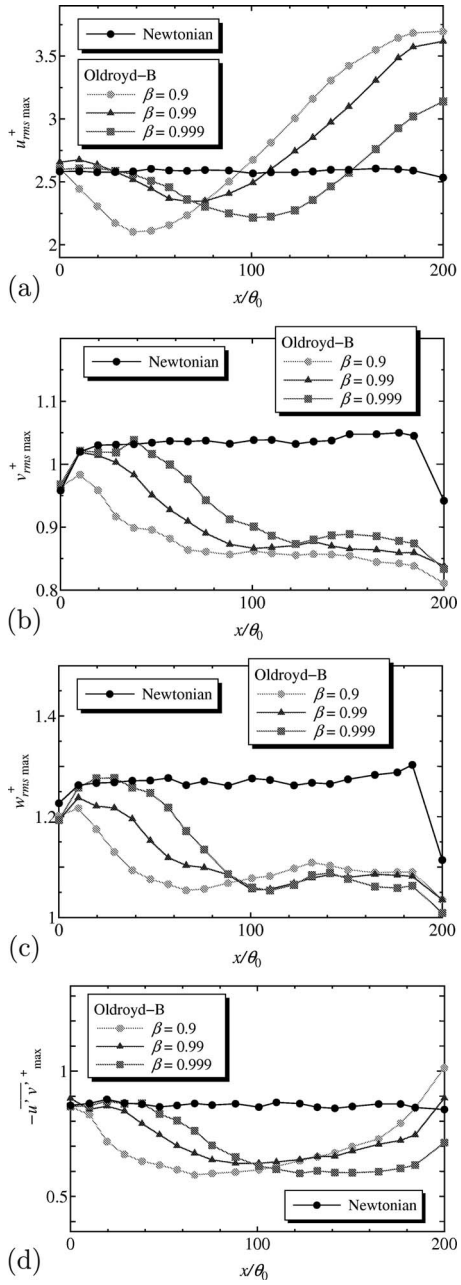

FIG. 10. Streamwise variations in local maxima of turbulence statistics for the Oldroyd-B model: (a) streamwise turbulence intensity, (b) wall-normal turbulence intensity, (c) spanwise turbulence intensity, and (d) Reynolds shear stress.

unrealistic behavior in the region very close to the outlet plane does not affect the present DNS results in the rest of the computational domain (see Appendix B for details). Figure 10(d) shows that the Reynolds shear stress $-\overline{u'v'}^{+}_{\max}$ for the Oldroyd-B model is much smaller than that for the Newtonian fluid. With the increase in β, $-\overline{u'v'}^{+}_{\max}$ increases in the region $x/\theta_0 < 100$, whereas it decreases in the region $x/\theta_0 > 100$, which does not correspond to the streamwise variation in DR. The reason for this is not known. However, the disagreement between the streamwise variations in DR and $-\overline{u'v'}^{+}_{\max}$ indicates that the drag-reducing turbulent boundary layer flow is more complex owing to the history effect of the

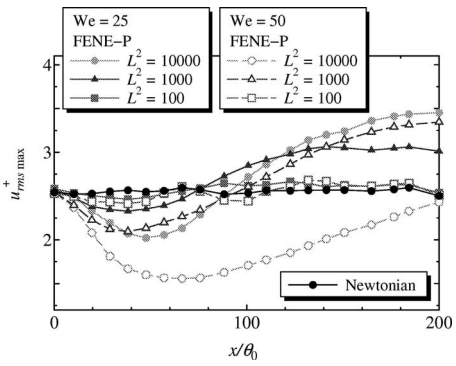

FIG. 11. Streamwise variation in local maximum of streamwise turbulence intensity at We=25 and 50 for the FENE-P model at β=0.9.

polymer-turbulence interaction compared to that for the turbulent channel flow, as noted in the DNS of Dimitropoulos *et al.*[2,3] and the experiment of Hou *et al.*[7]

To clarify the effect of rheological differences on the asynchronous behavior between the DR and turbulence statistics is helpful for understanding the drag-reducing mechanism in the turbulent boundary layer. Dimitropoulos *et al.*[2] reported that the phase difference between polymer stretch and vortex damping increased with elasticity, i.e., the Weissenberg number. Comparison between Figs. 2 and 10(a) indicates that the phase difference between DR and $u^{+}_{\mathrm{rms\ max}}$ increases with the increase in β, which corresponds to the increase in the retardation time λ'. Figure 11 shows the streamwise variation in $u^{+}_{\mathrm{rms\ max}}$ at We=25 and 50 for the FENE-P model at β=0.9. Comparing Figs. 9 and 11, it is found that at the same L^2, the phase difference between DR and $u^{+}_{\mathrm{rms\ max}}$ increases with the increase in We, which corresponds to the increase in the relaxation time λ. This is consistent with the first DNS of Dimitropoulos *et al.*[2] At the same We, the phase difference also increases with the increase in L^2, which corresponds to the increase in the maximum extension of polymer.

G. Relation between DR and trace of viscoelastic stress component

To discuss the relation between the streamwise variations in DR and the trace of the viscoelastic stress component $(1-\beta)\overline{E_{kk}}^{+}$, which represents the magnitude of the polymer elongation,[4] we focus on the local maximum of the trace of the viscoelastic stress components $(1-\beta)\overline{E_{kk}}^{+}_{\max}$. Figure 12 shows the streamwise variation in $(1-\beta)\overline{E_{kk}}^{+}_{\max}$ for the Oldroyd-B model. In Fig. 12, $(1-\beta)\overline{E_{kk}}^{+}_{\max}$ is not plotted at the inlet plane, since the data on the Newtonian fluid are directly given there in the present simulation. We performed the DNS under the numerical condition that the constitutive equation was solved at the inlet plane after imposing the Newtonian flow field data as the inlet boundary condition and confirmed that for such a case, the streamwise variation in $(1-\beta)\overline{E_{kk}}^{+}_{\max}$ in the region close to the inlet plane was very small, and the difference in the inlet boundary condition hardly affects the streamwise variation in DR (not shown here). The value of $(1-\beta)\overline{E_{kk}}^{+}_{\max}$ at β=0.9 gradually decreases from near the inlet to x/θ_0=140 and then slightly

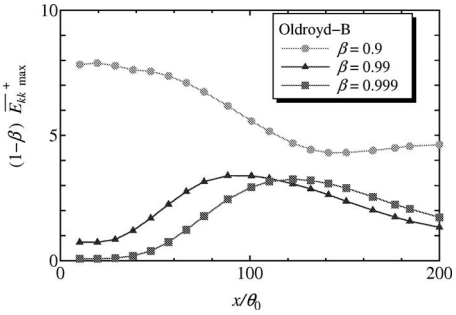

FIG. 12. Streamwise variation in local maximum of trace of viscoelastic stress components for the Oldroyd-B model.

increases in the streamwise direction. Near the inlet region, in which DR at $\beta=0.9$ is negative, $(1-\beta)\overline{E_{kk}}^{+}_{\max}$ is large. This can be explained as follows. Polymers are in equilibrium with the mean shear at the inlet and then experience a sudden increase in hydrodynamic forces due to the addition of turbulence. This obviously creates the opportunity for the high extensional viscosity; thus $(1-\beta)\overline{E_{kk}}^{+}_{\max}$ is large near the inlet region. The high extensional viscosity is going to have a dramatic impact on the flow, so that the skin friction drag increases near the inlet region.

Near the outlet region, in which DR is almost the maximum, $(1-\beta)\overline{E_{kk}}^{+}_{\max}$ is small. The present result supports the DNS of Dimitropoulos *et al.*[2,3] and the experiment of Hou *et al.*[7] Dimitropoulos *et al.*[2,3] first found that the development of polymer stretch and streamwise vortices was asynchronous, which was confirmed by DR increasing as polymer extension decreases. Dimitropoulos *et al.*[2] and Hou *et al.*[7] also presented the hypothetical mechanism that in the steady-state region, the reduced turbulent intensity allowed the polymer to be less stretched and still maintain a high DR, so that the polymer stress was not necessarily high. At $\beta=0.99$, DR around the center of the computational domain increases in the streamwise direction, while $(1-\beta)\overline{E_{kk}}^{+}_{\max}$ decreases. At $\beta=0.99$, $(1-\beta)\overline{E_{kk}}^{+}_{\max}$ becomes maximum near the center of the computational domain. At $\beta=0.999$, the streamwise variation in $(1-\beta)\overline{E_{kk}}^{+}_{\max}$ is similar to that at $\beta=0.99$, but the maximum is located more downstream. At $\beta=0.99$ and 0.999, from near the inlet to the center of the computational domain, $(1-\beta)\overline{E_{kk}}^{+}_{\max}$ becomes gradually larger owing to the interaction between polymer and turbulence, and then DR becomes larger with the phase lag (cf. Figs. 2 and 12). Further downstream, the larger viscoelastic stress is not necessary for maintaining the large DR, so that $(1-\beta)\overline{E_{kk}}^{+}_{\max}$ decreases gradually. The streamwise variations in $(1-\beta)\overline{E_{kk}}^{+}_{\max}$ at $\beta=0.99$ and 0.999 are fairly different from that at $\beta=0.9$. This is due to the difference in the wall-normal profiles of $(1-\beta)\overline{E_{kk}}^{+}$ among $\beta=0.9$, 0.99 and 0.999 (not shown here). As described above, the change in velocity fields near the inlet boundary is relatively small at $\beta=0.99$ and 0.999 which are very close to the Newtonian value ($\beta=1$), so that $(1-\beta)\overline{E_{kk}}^{+}_{\max}$ is small near the inlet region.

Comparison between Figs. 2 and 12 reveals that there is no distinct relation between the streamwise variations in DR and $(1-\beta)\overline{E_{kk}}^{+}_{\max}$ for the Oldroyd-B model. The same trend is also observed for the FENE-P and Giesekus models (not shown here). It was reported in Refs. 2, 4, and 7 that a direct relationship between the polymer stress and DR could not be observed for the drag-reducing turbulent boundary layer flow. The idea that there was a phase lag associated with the polymer activity as it responded to the turbulence and this phase difference allowed the possibility of the large DR with the low polymer stress was presented. The present DNS supports the idea[2,3,7] that there is a phase difference between DR and the viscoelastic stress and reveals that the relation between them is fairly complex.

V. CONCLUSIONS

DNS of a zero-pressure gradient drag-reducing turbulent boundary layer of viscoelastic fluids was systematically performed at the momentum-thickness Reynolds number $\mathrm{Re}_{\theta_0}=500$ and Weissenberg number $\mathrm{We}=25$ using constitutive equation models such as the Oldroyd-B model, the FENE-P model at the maximum chain extensibility parameters $L^2=100$, 1000, and 10 000, and the Giesekus model at the mobility factors $\alpha=0.01$, 0.001, and 0.0001, where the ratios of solvent viscosity to zero shear rate solution viscosity β were 0.9, 0.99, and 0.999. The effects of rheological properties such as the elongational viscosity, shear viscosity, and the first and the second normal stress differences on the streamwise variation in the DR were investigated, focusing on the case that the elongational viscosity for the steady elongational flow was identical, since the elongational viscosity was the most important rheological property for DR. To this end, two kinds of approaches were proposed as described in Appendix A.

It is revealed that the streamwise profile of DR shifts downstream with the decrease in the first normal stress difference, which corresponds to the increase in the retardation time λ'. The shear-thinning property and the first normal stress difference slightly affect the maximum DR. The decrease in the magnitude of the second normal stress difference results in the decrease in the maximum DR. It is also confirmed that at the higher Weissenberg number $\mathrm{We}=50$, in which the maximum DR is much larger, the effects of rheological properties on the streamwise variation in DR are qualitatively the same as those at $\mathrm{We}=25$. The streamwise profile of DR shifts downstream with the increase in We, which corresponds to the increase in the relaxation time λ.

The streamwise variation in the local maximum of the streamwise turbulence intensity $u^{+}_{\mathrm{rms}\ \max}$ seems to be related to that of DR, although the streamwise location of the onset of DR is more upstream compared to the location at which $u^{+}_{\mathrm{rms}\ \max}$ becomes larger than that for the Newtonian fluid, so that the direct relation between $u^{+}_{\mathrm{rms}\ \max}$ and DR is not observed at the same streamwise location. The phase difference between DR and $u^{+}_{\mathrm{rms}\ \max}$ increases with the increase in both the relaxation and retardation times in addition to the maximum extension of polymer. A direct relationship between DR and the viscoelastic stress cannot be observed for the drag-reducing turbulent boundary layer flow, which supports the previous numerical and experimental studies.[2,3,7]

Given the present macroscopic approach focused on the same elongational viscosity, which is based on steady rheo-

logical properties such as elongational and shear viscosities and the first and the second normal stress differences, considerable new knowledge could be obtained. For further investigation of the drag-reducing mechanism, however, it would be required to clarify the effect of the transient response for each constitutive equation model on the streamwise variation in the DR. In addition, it remains unknown how polymers or surfactant micelles interact with the near-wall turbulence structures and how unsteady rheological properties play a role in DR in the turbulent boundary layer flow. For further understanding of the mechanism of DR, a microscopic approach would also be required. To this end, the Brownian dynamic simulations[28,29] for the drag-reducing turbulent boundary layer flow may be one of the promising candidates.

ACKNOWLEDGMENTS

This work was partially carried out under the ISM Cooperative Research Program. It was partially supported by a Grant-in-Aid for Scientific Research (Grant No. 18360087) from the Japan Society for the Promotion of Science.

APPENDIX A: RHEOLOGICAL PROPERTIES FOR STEADY ELONGATIONAL AND SHEAR FLOWS

For comparison of the DNS data for the case that the elongational viscosity is identical or almost the same, two kinds of approaches could be considered for the constitutive equation models such as the Oldroyd-B, FENE-P, and Giesekus models. One approach is as follows: for each constitutive equation model, the shear viscosity ratio β, the maximum extension L^2, and the mobility factor α are altered under various combinations of β, L^2, and α (see Secs. IV A–IV C for details). Another approach is as follows: at the constant β, the combinations of L^2 and α are altered while satisfying a relation between L^2 and α for the FENE-P and Giesekus models (details in Sec. IV D). Regarding the former approach, the elongational viscosity is identical when $(1-\beta)L^2$ is constant for the FENE-P model. For the Giesekus model, the constant $(1-\beta)/\alpha$ results in the identical elongational viscosity. For the Oldroyd-B model, the elongational viscosity is inherently almost the same for different β. Regarding the latter approach, the elongational viscosity for both the FENE-P and Giesekus models becomes identical at the condition of $\alpha=1/L^2$. In the following, we present the rheological properties for the Oldroyd-B, FENE-P, and Giesekus models.

In the present study, η_E is the elongational viscosity for the steady elongational flow. For the Oldroyd-B model,[26] $\eta_E/(3\eta_0)$ is represented by

$$\frac{\eta_E}{3\eta_0} = \beta + \frac{1-\beta}{(1+\xi)(1-2\xi)}, \tag{A1}$$

where $\xi=\lambda\dot{\varepsilon}$ is the nondimensional elongational rate.

For the FENE-P model,[26,30–32] the elongational viscosity $\eta_E/(3\eta_0)$ is given by

$$\frac{\eta_E}{3\eta_0} = \beta + \frac{(1-\beta)L^2\phi}{3}, \tag{A2}$$

where ϕ is obtained by solving the following equation:

$$\phi^3 + P\phi^2 + Q\phi + R = 0, \tag{A3}$$

where P, Q, and R are

$$P = \frac{1}{2}\left(\frac{L^2+3}{L^2\xi} - 5\right),$$

$$Q = 1 - \frac{1}{2L^2\xi}\left(3 - L^2 + \frac{3+L^2}{\xi}\right), \tag{A4}$$

$$R = \frac{3}{2L^2\xi^2}.$$

For the Giesekus model,[26] the elongational viscosity $\eta_E/(3\eta_0)$ is represented as follows:

$$\frac{\eta_E}{3\eta_0} = \beta + \frac{1-\beta}{6\alpha\xi}\left[\sqrt{1-4(1-2\alpha)\xi+4\xi^2} - \sqrt{1+2(1-2\alpha)\xi+\xi^2}+3\xi\right]. \tag{A5}$$

In the present study, η, $\psi_1=(\tau_{11}-\tau_{22})/\dot{\gamma}^2$, and $\psi_2=(\tau_{22}-\tau_{33})/\dot{\gamma}^2$ are the shear viscosity and the first and the second normal stress difference coefficients for the steady shear flow, respectively. For the Oldroyd-B model,[24] η/η_0, ψ_1, and ψ_2 are represented as follows:

$$\frac{\eta}{\eta_0} = 1, \tag{A6}$$

$$\psi_1 = 2\lambda\eta_0(1-\beta), \tag{A7}$$

$$\psi_2 = 0. \tag{A8}$$

For the FENE-P model,[26,30–32] η/η_0, ψ_1, and ψ_2 are represented by

$$\frac{\eta}{\eta_0} = \beta + \frac{(1-\beta)}{\kappa}\left[(C_2+C_1)^{1/3} - (C_2-C_1)^{1/3}\right], \tag{A9}$$

$$\psi_1 = \frac{2\eta_p}{\kappa\dot{\gamma}}\left[(C_2+C_1)^{1/3} - (C_2-C_1)^{1/3}\right]^2, \tag{A10}$$

$$\psi_2 = 0, \tag{A11}$$

where $\kappa=\lambda\dot{\gamma}$ is the nondimensional shear rate and C_1 and C_2 are

$$C_1 = \frac{L^2\kappa}{4}, \tag{A12}$$

$$C_2 = \sqrt{\left(\frac{L^2\kappa}{4}\right)^2 + \left(\frac{L^2+3}{6}\right)^3}. \tag{A13}$$

For the Giesekus model,[26] η/η_0, ψ_1, and ψ_2 are given by

$$\frac{\eta}{\eta_0} = \beta + \frac{(1-\beta)(1-n_2)^2}{1+(1-2\alpha)n_2}, \tag{A14}$$

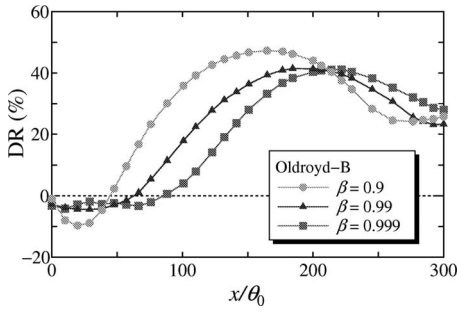

FIG. 13. Streamwise variation in DR for the Oldroyd-B model with $L_x/\theta_0 = 300$.

$$\psi_1 = \frac{2n_2\eta_0(1-\beta)(1-\alpha n_2)}{\kappa^2\alpha(1-n_2)}, \tag{A15}$$

$$\psi_2 = -\frac{n_2\eta_0(1-\beta)}{\kappa^2}, \tag{A16}$$

where n_2 is

$$n_2 = \frac{1-\Lambda}{1+(1-2\alpha)\Lambda}. \tag{A17}$$

Here, Λ is given by the following equation:

$$\Lambda^2 = \frac{\sqrt{1+16\alpha(1-\alpha)\kappa^2}-1}{8\alpha(1-\alpha)\kappa^2}. \tag{A18}$$

APPENDIX B: EFFECT OF THE SIZE OF THE STREAMWISE COMPUTATIONAL DOMAIN

In order to investigate the effects of the size of the streamwise computational domain, we performed a DNS of the turbulent boundary layer in a 1.5 times larger streamwise computational domain ($L_x/\theta_0 = 300$), in which the other computational parameters are the same except for the larger streamwise grid number ($N_x = 384$) to keep the same grid resolution.

Figure 13 shows the streamwise variation in DR for the Oldroyd-B model with $L_x/\theta_0 = 300$. It is found that the streamwise variation in DR shifts downstream with the increase in β, as shown in Fig. 2 with $L_x/\theta_0 = 200$, although at $\beta = 0.9$, the maximum DR with $L_x/\theta_0 = 300$ is somewhat larger than that with $L_x/\theta_0 = 200$. This means that the present size of the streamwise computational domain is enough for the present rheological analysis, except for the quantitative investigation of the maximum DR.

Figures 14(a)–14(d) show the streamwise variations in $u^+_{\mathrm{rms\ max}}$, $v^+_{\mathrm{rms\ max}}$, $w^+_{\mathrm{rms\ max}}$, and $-\overline{u'v'}^+_{\max}$ for the Oldroyd-B model with $L_x/\theta_0 = 300$. It is found that the streamwise variations in turbulence statistics with $L_x/\theta_0 = 300$ are almost the same as those with $L_x/\theta_0 = 200$ in the region $x/\theta_0 < 200$, as compared with Figs. 10(a)–10(d). Therefore, we can conclude that the unrealistic behavior in the region very close to the outlet plane does not affect the turbulence statistics in the rest of the computational domain. It is found that $-\overline{u'v'}^+_{\max}$ is larger than that for the Newtonian fluid in the region $x/\theta_0 > 200$. This may be due to the difference in $u^+_{\mathrm{rms\ max}}$ between the Oldroyd-B model and the Newtonian fluid.

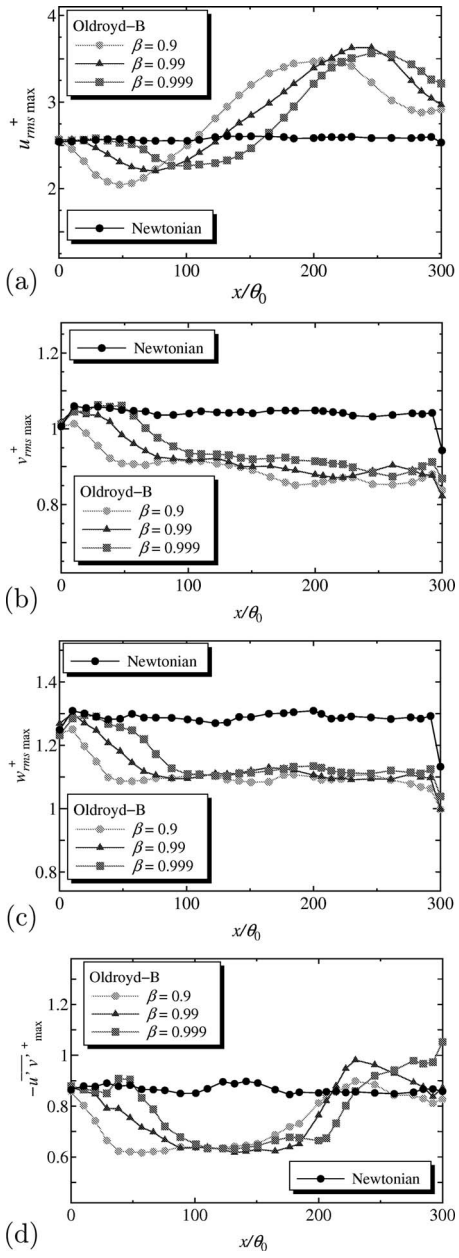

FIG. 14. Streamwise variations in local maxima of turbulence statistics for the Oldroyd-B model with $L_x/\theta_0 = 300$: (a) streamwise turbulence intensity, (b) wall-normal turbulence intensity, (c) spanwise turbulence intensity, and (d) Reynolds shear stress.

Figure 15 shows the streamwise variations in DR at We=25 and 50 for the FENE-P model at $L^2 = 10\,000$ and $\beta = 0.9$ with $L_x/\theta_0 = 300$. Comparing Fig. 9 with Fig. 15, it is confirmed that at both We=25 and 50, the streamwise variations with $L_x/\theta_0 = 300$ are almost the same as those with $L_x/\theta_0 = 200$ in the region $x/\theta_0 < 200$. On the other hand, the maximum DR at We=50 with $L_x/\theta_0 = 300$ grows to DR = 64%, which is larger than that with $L_x/\theta_0 = 200$ and slightly larger than that of Dimitropoulos *et al.*[2] at the same Weissenberg number, while at We=25, no distinct difference in the maximum DR can be observed between $L_x/\theta_0 = 200$ and 300. This indicates that for the FENE-P model at $L^2 = 10\,000$, the

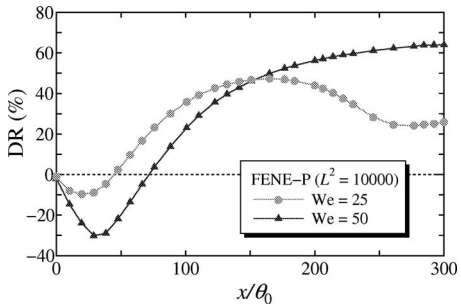

FIG. 15. Streamwise variations in DR at We=25 and 50 for the FENE-P model at L^2=10 000 and β=0.9 with L_x/θ_0=300.

present streamwise computational domain of L_x/θ_0=200 is somewhat small at We=50 for discussing the maximum DR correctly. This is also supported by the study of Li *et al.*,[20] who reported that a larger computational domain was needed for reliable DNS of the turbulent channel flow with a larger friction Weissenberg number, i.e., a larger DR. For the DNS of the turbulent boundary layer with large DR, how far and whether a stationary value will be attained are still open questions.

[1] C. M. White and M. G. Mungal, "Mechanics and prediction of turbulent drag reduction with polymer additives," Annu. Rev. Fluid Mech. **40**, 235 (2008).
[2] C. D. Dimitropoulos, Y. Dubief, E. S. G. Shaqfeh, P. Moin, and S. K. Lele, "Direct numerical simulation of polymer-induced drag reduction in turbulent boundary layer flow," Phys. Fluids **17**, 011705 (2005).
[3] C. D. Dimitropoulos, Y. Dubief, E. S. G. Shaqfeh, and P. Moin, "Direct numerical simulation of polymer-induced drag reduction in turbulent boundary layer flow of inhomogeneous polymer solutions," J. Fluid Mech. **566**, 153 (2006).
[4] S. Tamano, M. Itoh, K. Hoshizaki, and K. Yokota, "Direct numerical simulation on the drag-reducing turbulent boundary layer of viscoelastic fluid," Phys. Fluids **19**, 075106 (2007).
[5] C. M. White, V. S. R. Somandepalli, and M. G. Mungal, "The turbulence structure of drag-reduced boundary layer flow," Exp. Fluids **36**, 62 (2004).
[6] M. Itoh, S. Tamano, K. Yokota, and M. Ninagawa, "Velocity measurement in turbulent boundary layer of drag-reducing surfactant solution," Phys. Fluids **17**, 075107 (2005).
[7] Y. X. Hou, V. S. R. Somandepalli, and M. G. Mungal, "Streamwise development of turbulent boundary-layer drag reduction with polymer injection," J. Fluid Mech. **597**, 31 (2008).
[8] S. Hofmann, P. Stern, and J. Myska, "Rheological behavior and birefringence investigations on drag-reducing surfactant solutions of tallow-(tris-hydroxyethyl)-ammonium acetate/sodiumsalicylate mixtures," Rheol. Acta **33**, 419 (1994).
[9] Y. Hu and E. F. Matthys, "Characterization of micellar structure dynamics for a drag-reducing surfactant solution under shear: Normal stress studies and flow geometry effects," Rheol. Acta **34**, 450 (1995).
[10] Y. Hu and E. F. Matthys, "The effects of salts on the rheological characteristics of a drag-reducing cationic surfactant solution with shear-induced micellar structures," Rheol. Acta **35**, 470 (1996).
[11] B. Lu, X. Li, J. L. Zakin, and Y. Talmon, "A non-viscoelastic drag reducing cationic surfactant system," J. Non-Newtonian Fluid Mech. **71**, 59 (1997).
[12] B. Lu, Y. Zheng, H. T. Davis, L. E. Scriven, Y. Talmon, and J. L. Zakin, "Effect of variations in counterion to surfactant ratio on rheology and microstructures of drag reducing cationic surfactant systems," Rheol. Acta **37**, 528 (1998).
[13] Z. Lin, Y. Zheng, H. T. Davis, L. E. Scriven, Y. Talmon, and J. L. Zakin, "Unusual effects of counterion to surfactant concentration ratio on viscoelasticity of a cationic surfactant drag reducer," J. Non-Newtonian Fluid Mech. **93**, 363 (2000).
[14] J. Wei, Y. Kawaguchi, B. Yu, and Z. Feng, "Rheological characteristics and turbulent friction drag and heat transfer reductions of a very dilute cationic surfactant solution," J. Heat Transfer **128**, 977 (2006).
[15] K. Vissmann and H.-W. Bewersdorff, "The influence of pre-shearing on the elongational behaviour of dilute polymer and surfactant solutions," J. Non-Newtonian Fluid Mech. **34**, 289 (1990).
[16] Y. Kawaguchi, J. Wei, B. Yu, and Z. Feng, "Rheological characterization of drag-reducing cationic surfactant solution-shear and elongational viscosities of dilute solutions," in *Proceedings of the Fourth ASME-JSME Joint Fluids Engineering Conference*, Honolulu, HI, 6–10 July 2003 (ASME, New York, 2003), Paper No. 45653.
[17] J. S. Paschkewitz, C. D. Dimitropoulos, Y. X. Hou, V. S. R. Somandepalli, M. G. Mungal, E. S. G. Shaqfeh, and P. Moin, "An experimental and numerical investigation of drag reduction in a turbulent boundary layer using a rigid rodlike polymer," Phys. Fluids **17**, 085101 (2005).
[18] C. D. Dimitropoulos, R. Sureshkumar, and A. N. Beris, "Direct numerical simulation of viscoelastic turbulent channel flow exhibiting drag reduction: Effect of the variation of rheological parameters," J. Non-Newtonian Fluid Mech. **79**, 433 (1998).
[19] K. D. Housiadas and A. N. Beris, "An efficient fully implicit spectral scheme for DNS of turbulent viscoelastic channel flow," J. Non-Newtonian Fluid Mech. **122**, 243 (2004).
[20] C.-F. Li, R. Sureshkumar, and B. Khomami, "Influence of rheological parameters on polymer induced turbulent drag reduction," J. Non-Newtonian Fluid Mech. **140**, 23 (2006).
[21] B. Yu and Y. Kawaguchi, "Parametric study of surfactant-induced drag-reduction by DNS," Int. J. Heat Fluid Flow **27**, 887 (2006).
[22] K. D. Housiadas and A. N. Beris, "Polymer-induced drag reduction: Effects of the variations in elasticity and inertia in turbulent viscoelastic channel flow," Phys. Fluids **15**, 2369 (2003).
[23] T. S. Lund, X. Wu, and K. D. Squires, "Generation of turbulent inflow data for spatially-developing boundary layer simulations," J. Comput. Phys. **140**, 233 (1998).
[24] J. K. Dukowicz and A. S. Dvinsky, "Approximate factorization as a high order splitting for the implicit incompressible flow equations," J. Comput. Phys. **102**, 336 (1992).
[25] H. A. Van Der Vorst, "Bi-CGSTAB: A fast and smoothly converging variant of BiCG for the solution of nonsymmetric linear systems," SIAM (Soc. Ind. Appl. Math.) J. Sci. Stat. Comput. **13**, 631 (1992).
[26] R. B. Bird, R. C. Armstrong, and O. Hassager, *Dynamics of Polymeric Liquids*, 2nd ed. (Wiley Interscience, New York, 1987), Vol. 1.
[27] M. Renardy, "On the mechanism of drag reduction," J. Non-Newtonian Fluid Mech. **59**, 93 (1995).
[28] P. A. Stone and M. D. Graham, "Polymer dynamics in a model of the turbulent buffer layer," Phys. Fluids **15**, 1247 (2003).
[29] V. E. Terrapon, Y. Dubief, P. Moin, E. S. G. Shaqfeh, and S. K. Lele, "Simulated polymer stretch in a turbulent flow using Brownian dynamics," J. Fluid Mech. **504**, 61 (2004).
[30] R. B. Bird, C. F. Curtiss, R. C. Armstrong, and O. Hassager, *Dynamics of Polymeric Liquids*, 2nd ed. (Wiley Interscience, New York, 1987), Vol. 2.
[31] R. B. Bird, P. J. Dotson, and N. L. Johnson, "Polymer solution rheology based on a finitely extensible bead-spring chain model," J. Non-Newtonian Fluid Mech. **7**, 213 (1980).
[32] M. E. Mackay and C. J. S. Petrie, "Estimates of apparent elongational viscosity using the fibre spinning and pure methods," Rheol. Acta **28**, 281 (1989).